Progression-associated molecular changes in basal/squamous and sarcomatoid bladder carcinogenesis

Jacqueline Fontugne, Jennifer Wong, Luc Cabel, Hélène Neyret-Kahn, Narjesse Karboul, Pascale Maillé, Audrey Rapinat, David Gentien, André Nicolas, Sylvain Baulande, et al.

Journal of Pathology
J Pathol April 2023; **259:** 455–467
Published online 24 February 2023 in Wiley Online Library
(wileyonlinelibrary.com) **DOI:** 10.1002/path.6060

ORIGINAL ARTICLE

Progression-associated molecular changes in basal/squamous and sarcomatoid bladder carcinogenesis

Jacqueline Fontugne[1,2,3], Jennifer Wong[1,4], Luc Cabel[1], Hélène Neyret-Kahn[1], Narjesse Karboul[1], Pascale Maillé[2], Audrey Rapinat[5], David Gentien[5], André Nicolas[6], Sylvain Baulande[7], Mathilde Sibony[8], Isabelle Bernard-Pierrot[1†], François Radvanyi[1†] and Yves Allory[1,2,3*†]

[1] *Institut Curie, CNRS, UMR144, Equipe labellisée Ligue Contre le Cancer, PSL Research University, Paris, France*
[2] *Department of Pathology, Institut Curie, Saint-Cloud, France*
[3] *Université Paris-Saclay, Université Versailles St-Quentin, Montigny-le-Bretonneux, France*
[4] *Department of Genetics, Institut Curie, Paris, France*
[5] *Genomics Core Facility, Translational Research Department, PSL Research University, Institut Curie, Paris, France*
[6] *Department of Pathology, Institut Curie, Paris, France*
[7] *Genomics of Excellence (ICGex) Platform, Institut Curie, PSL Research University, Paris, France*
[8] *Department of Pathology, Hôpital Cochin, Paris, France*

**Correspondence to: Y Allory, Département de Pathologie/UMR 144, Équipe Oncologie Moléculaire, Institut Curie – Site Saint Cloud, 35 Rue Dailly, 92210 Saint-Cloud, France. E-mail: yves.allory@curie.fr*

†These authors co-supervised the study.

Abstract

The aggressive basal/squamous (Ba/Sq) bladder cancer (BLCA) subtype is often diagnosed at the muscle-invasive stage and can progress to the sarcomatoid variant. Identification of molecular changes occurring during progression from non-muscle-invasive BLCA (NMIBC) to Ba/Sq muscle-invasive BLCA (MIBC) is thus challenging in human disease. We used the *N*-butyl-*N*-(4-hydroxybutyl)-nitrosamine (BBN) mouse model of Ba/Sq MIBC to study longitudinally the molecular changes leading to the Ba/Sq phenotype and to the sarcomatoid variant using IHC and microdissection followed by RNA-seq at all stages of progression. A shift to the Ba/Sq phenotype started in early progression stages. Pathway analysis of gene clusters with coordinated expression changes revealed Shh signaling loss and a shift from fatty acid metabolism to glycolysis. An upregulated cluster, appearing early in carcinogenesis, showed relevance to human disease, identifying NMIBC patients at risk of progression. Similar to the human counterpart, sarcomatoid BBN tumors displayed a Ba/Sq phenotype and epithelial–mesenchymal transition (EMT) features. An EGFR/FGFR1 signaling switch occurred with sarcomatoid dedifferentiation and correlated with EMT. BLCA cell lines with high EMT were the most sensitive to *FGFR1* knockout and resistant to *EGFR* knockout. Taken together, these findings provide insights into the underlying biology of Ba/Sq BLCA progression and sarcomatoid dedifferentiation with potential clinical implications.

Keywords: urothelial carcinoma; carcinogenesis; molecular evolution of bladder cancer; immunohistochemistry; sarcomatoid variant; EGFR; FGFR1; BBN mouse model

Received 5 August 2022; Revised 13 December 2022; Accepted 23 January 2023

No conflicts of interest were declared.

Introduction

Bladder cancer (BLCA) is the tenth most common cancer type worldwide, and caused nearly 200,000 deaths in 2018 [1]. The vast majority of BLCAs are urothelial carcinomas, characterized by two clinically distinct forms of disease [2]. Non-muscle-invasive bladder cancer (NMIBC) – papillary pTa, flat carcinoma *in situ* (CIS), and pT1 stage tumors – often recur, leading to a significant burden on patients' quality of life [3]. In contrast, muscle-invasive bladder cancer (MIBC, ≥pT2) represents the lethal form of disease. Most patients with MIBC show no history of precursor NMIBC, challenging the study of carcinogenesis and progression in human disease. Overlaps in genomic alterations and lineage tracing studies in mice suggest that CIS represents a major precursor of MIBCs [4–6]. However, the precise relationships between the different forms of NMIBC and MIBC have not been fully elucidated.

Transcriptomic classifications identified molecular subtypes of MIBC, with different clinical characteristics [7–11]. The major molecular subtypes distinguish

luminal subtypes and the basal/squamous (Ba/Sq) subtype. The consensus Ba/Sq subtype of MIBC is a frequent (~35%) and aggressive subtype with poor survival. Histologically, nearly half of Ba/Sq MIBCs harbor squamous divergence and may eventually progress to the aggressive sarcomatoid variant, often composed of tumor cells of spindle morphology [12–14]. Tumors of the Ba/Sq phenotype can be accurately identified by the combined overexpression of basal (KRT5, KRT6, KRT14) and underexpression of luminal cell markers (FOXA1, GATA3), including by immunohistochemistry [8,15,16]. They display high EGFR activity, with EGFR dependence *in vitro* and *in vivo* [7,17]. Since most NMIBCs are considered to display a luminal phenotype, and the vast majority of carcinomas *in situ* show aberrant high expression of KRT20, one could assume that a subtype switch is required during the progression from NMIBC to Ba/Sq MIBC [18]. However, Ba/Sq tumors are often diagnosed at the muscle-invasive stage, rarely preceded by NMIBC tumors, hindering the longitudinal study of molecular alterations from early-stage carcinoma to Ba/Sq MIBC [17,19].

N-Butyl-*N*-(4-hydroxybutyl)-nitrosamine (BBN) carcinogen specifically induces bladder tumors in mice and represents an attractive model of MIBC [20]. We and others have demonstrated that BBN-induced MIBC is a model of the Ba/Sq transcriptomic subtype and can harbor squamous divergence, or more rarely sarcomatoid features [17,21]. We thus hypothesized that the BBN-induced model represents a stable means to longitudinally study Ba/Sq BLCA progression.

In this study, we aimed to identify the molecular changes occurring during the carcinogenesis of Ba/Sq MIBC. We report histological, immunohistochemical, and RNA-seq profiles of lesions of all stages of progression in a carcinogen-induced murine model of the Ba/Sq subtype of MIBC. We showed that early-stage tumors already displayed Ba/Sq features and identified sets of genes with coordinated changes during progression. One cluster of co-expressed genes, which increased early in Ba/Sq MIBC carcinogenesis, showed relevance to human tumors, identifying patients with NMIBC at risk of progression. A focus on BBN-induced sarcomatoid tumors showed similarities with the human counterpart, such as epithelial–mesenchymal transition features, and revealed that an EGFR to FGFR1 signaling switch occurs with sarcomatoid dedifferentiation, with potential therapeutic implications.

Materials and methods

Study approval

Animal experiments were performed in accordance with recommendations of the European Community (2010/63/UE) for the care and use of laboratory animals. Experimental procedures were approved by the Ethics Committee of Institut Curie CEEA-IC #118 (Authorization APAFiS #26671-2,020,072,108,262,352-v2 given by National Authority) in compliance with international guidelines.

BBN-induced mouse model

Forty 8-week-old male C57BL/6 mice were exposed to *N*-butyl-*N*-(4-hydroxybutyl)-nitrosamine (BBN) 0.05% in drinking water *ad libitum* for a maximum of 14 weeks. Mice were sacrificed at different time points to obtain tumors of all stages. Five control mice received non-treated drinking water. Details are provided in Supplementary materials and methods.

Tissue processing

Mouse bladders were formalin-fixed, paraffin-embedded (FFPE) and then sectioned at 3-µm thickness. Slides at three different levels were stained with hematoxylin, eosin, and saffron (HES) for morphological analysis, and ten unstained slides from flanking sections between each level were reserved at 4 °C for immunohistochemistry.

Immunohistochemistry

Immunohistochemistry (IHC) for luminal and basal markers, using rabbit polyclonal antibodies to KRT5, KRT6A, KRT14, FOXA1, and KRT20, and for the proliferation marker Ki67 was performed on an Autostainer 480 (Lab Vision; Thermo Fisher Scientific, Waltham, MA, USA). Subtype markers were quantified using a quick score method [17]. Vimentin IHC was performed on a subset of cases, using a rabbit monoclonal anti-vimentin antibody. Details are provided in Supplementary materials and methods.

Morphological analysis

The three levels of HES-stained slides per case and IHC subtype markers were reviewed by uropathologists (JF, MS, YA). The highest-stage lesion for each mouse bladder was documented regarding the presence of variant morphology and stage according to the WHO 2016 classification of urothelial tumors and TNM 8th edition UICC staging [2] (Supplementary materials and methods). In two cases harboring several lesions of identical stage with discordant IHC profiles, each lesion was documented individually regarding the aforementioned morphological parameters.

Tissue microdissection

Large MIBC tumors ($n = 3$) were manually microdissected by scraping five 6-µm-thick sections with visual control under a stereomicroscope, using the corresponding HES-stained slide for reference. For all other cases, we performed laser-capture microdissection (LMD7000; Leica Microsystems, Wetzlar, Germany) (see Supplementary materials and methods).

RNA extraction, library preparation, and sequencing

RNA was extracted from microdissected BBN-induced lesions and non-exposed urothelia using an RNeasy FFPE Kit (Qiagen, Hilden, Germany). Libraries were prepared using the Ovation SoLo RNA-Seq System (NuGEN/Tecan, Männedorf, Switzerland) and sequenced on a HiSeq 2500 (Illumina, San Diego, CA, USA). Reads were mapped to the mouse reference genome (mm10) using STAR (version 2.6.1a) [22] and counted with Rsubread (version 1.24.2) [23] (see Supplementary materials and methods).

Identification of sample groups

Principal component analysis (PCA) was performed using the prcomp function in R [24]. Unsupervised clustering iterations were performed using the ConsensusClusterPlus R package (v1.48.0) [25] (see Supplementary materials and methods).

Sample molecular classification

Mouse samples were classified using corresponding human homolog genes, obtained using the biomaRt R package (v2.40.5, genome assemblies GRCm38.p6 and GRCh38.p13) [26]. Lund taxonomy (LundTax) and BASE47 classes were obtained using BLCAsubtyping (v2.1.1) [7]. Consensus subtypes were determined with the ConsensusMIBC (v1.1.0) R package [7]. The UROMOL study NMIBC classes were obtained using the online application [27].

Gene expression changes during progression

To identify significant expression changes during progression, we used an R package designed for RNA-seq time-course data, Next maSigPro (v1.56.0) (see Supplementary materials and methods). Genes with significant temporal changes were clustered into $k = 2$ to $k = 8$ solutions. Functional enrichment was evaluated in each k solution using the clusterProfiler (v3.12.0) [28] and ReactomePA (v1.28.0) [29] R packages. The lowest k solution capturing the most patterns of co-expression changes and grouping biologically related genes was selected as the final clustering solution ($k = 5$).

Differential gene expression analyses

Pairwise differentially expressed genes were determined using DESeq2 (v1.24.0) [30] in the BBN RNA-seq data, and Limma (v3.40.6) [31]package for array expression profiling data of human sarcomatoid cases from Guo *et al* [12] (see Supplementary materials and methods).

Epithelial–mesenchymal transition (EMT) scores

We used a previously published signature combining 206 epithelial and 132 mesenchymal genes [32]. EMT scores were calculated by subtracting the mean log2-normalized expression of the epithelial from that of the mesenchymal genes in each sample.

Regulon activity

In our BBN and in the Guo *et al* cohorts, we determined the activity of 22 regulators reported to play a role in BLCA, as previously described [11] (see also Supplementary materials and methods).

Statistical analysis

Details are provided in Supplementary materials and methods.

Results

BBN-exposed mice develop the full tumor spectrum of bladder carcinogenesis

To study disease progression, 40 mice were exposed to BBN and sacrificed at different time points (Figure 1A). As previously described [33], histopathological analysis of mouse bladders after increasing durations of BBN exposure revealed a spectrum of lesions, including hyperplasia, dysplasia, CIS, papillary pTa, pT1, and muscle-invasive tumors, confirming that the model progresses along stages similar to those found in human urothelial carcinogenesis (Figure 1B–E) [2]. Flat neoplastic lesions (Figure 1B and supplementary material, Figure S1) and high-grade papillary pTa tumors (Figure 1C) arose at week 8 and week 12, respectively. Infiltrating carcinoma, defined hereafter as breaching the basement membrane, was seen starting from week 12 and involved the lamina propria (pT1) or the bladder muscle (MIBC) (Figure 1D). Most infiltrating tumors showed squamous differentiation (Figure 1D,F). However, four infiltrating tumors lacked squamous features and displayed spindle morphology, suggestive of the sarcomatoid variant of human urothelial carcinoma (Figure 1D,F and supplementary material, Figure S1C).

Distinct transcriptomic groups reflect histological stages of progression

We performed laser-capture microdissection (supplementary material, Figure S2) followed by RNA sequencing of 37 samples, including 29 lesions from 27 BBN-exposed mice, representative of all stages of carcinogenesis: hyperplasia ($n = 4$), dysplasia ($n = 5$), CIS ($n = 3$), pTa ($n = 5$), pT1 ($n = 7$), and MIBC ($n = 5$). We also sequenced three BBN-exposed urothelia of normal morphology and five unexposed control urothelia. To assess the transcriptomic similarity between samples, we performed PCA, which showed a separation of samples according to stage and differentiation along the first and the second component, respectively (Figure 2A). To further confirm that progression groups were related to morphological stage, unsupervised clustering iteration was performed [25]. The $k = 3$ clustering solution was the most robust in all tested clustering and linkage methods (Figure 2B,C). The three clusters were associated with stage, essentially grouping (1) normal and premalignant

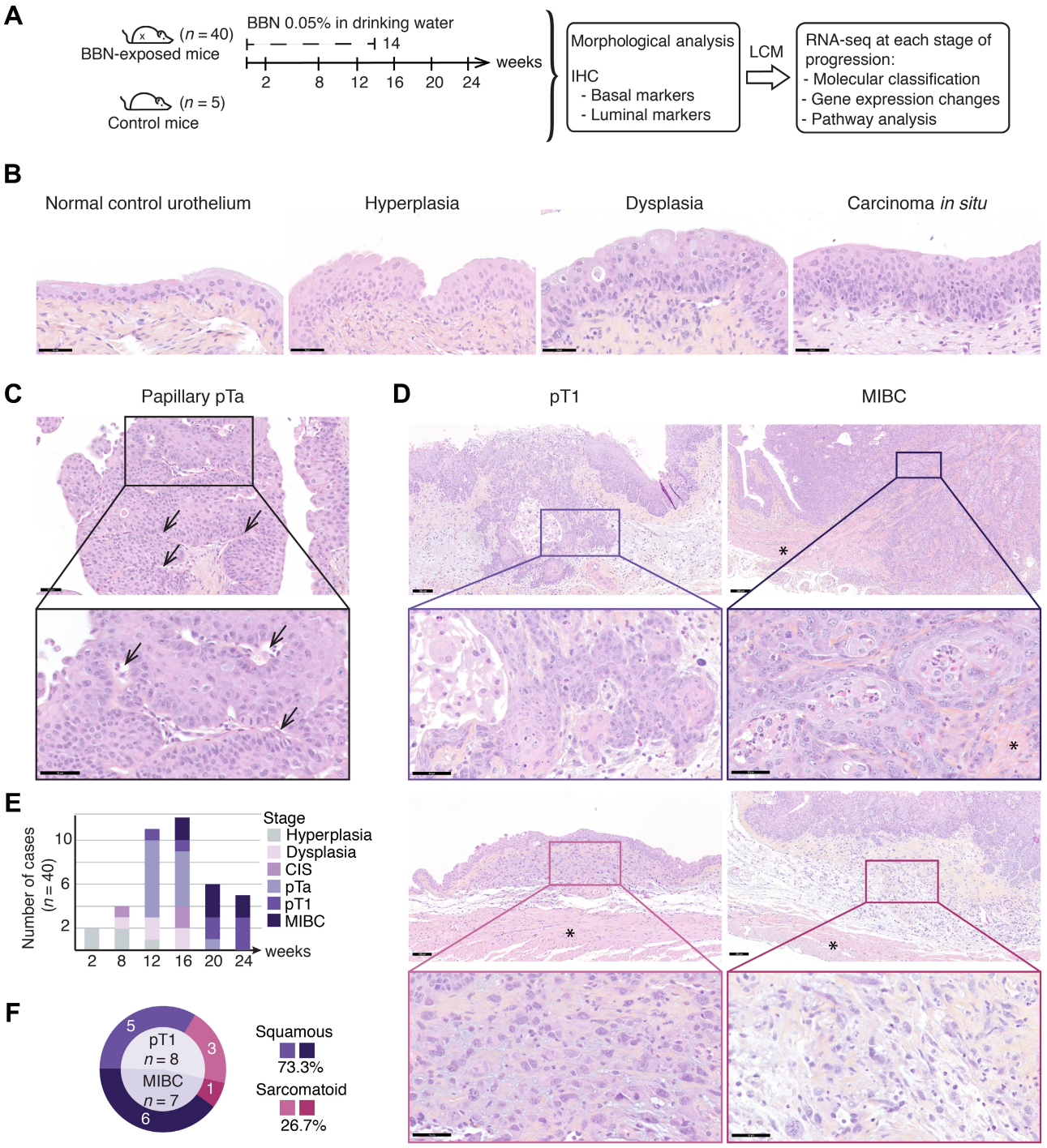

Figure 1. Mice develop a spectrum of bladder lesions with increasing BBN exposure, comparable to human carcinogenesis. (A) Study design and workflow: 40 mice were exposed to BBN for a maximum of 14 weeks and sacrificed at different time points. The highest-stage lesions in each bladder were morphologically and immunohistochemically characterized. RNA-seq was performed on a subset of cases of all stages of progression following laser-capture microdissection. Five non-exposed mice were used as controls. (B–D) Representative hematoxylin, eosin, saffron-stained images of the spectrum of lesions identified during BBN exposure: flat hyperplasia, dysplasia, and carcinoma *in situ* (B); papillary pTa tumors (C); and infiltrating tumors (D). (B) A normal untreated control urothelial is shown for reference. Infiltrating tumors either harbored areas of squamous differentiation (purple insets) or had pure sarcomatoid morphology (pink insets). Scale bars: 50 µm. Arrows point to papillary axes. Asterisks indicate bladder muscle. (E) Total number of each lesion type according to the time point of sacrifice after the start of BBN exposure, reporting the highest-stage lesion in each bladder. (F) Proportion of squamous or sarcomatoid differentiation in all observed infiltrating cases. BBN, *N*-butyl-*N*-(4-hydroxybutyl)-nitrosamine; LCM, laser-capture microdissection; MIBC, muscle-invasive bladder cancer.

stages, (2) early neoplastic stages, and (3) infiltrating stages (pT1 and MIBCs). Interestingly, higher *k* solutions further divided the infiltrating group according to differentiation (squamous versus sarcomatoid), regardless of stage (pT1 or MIBC) (Figure 2D). The sarcomatoid variant is suggested to develop by progression of conventional basal

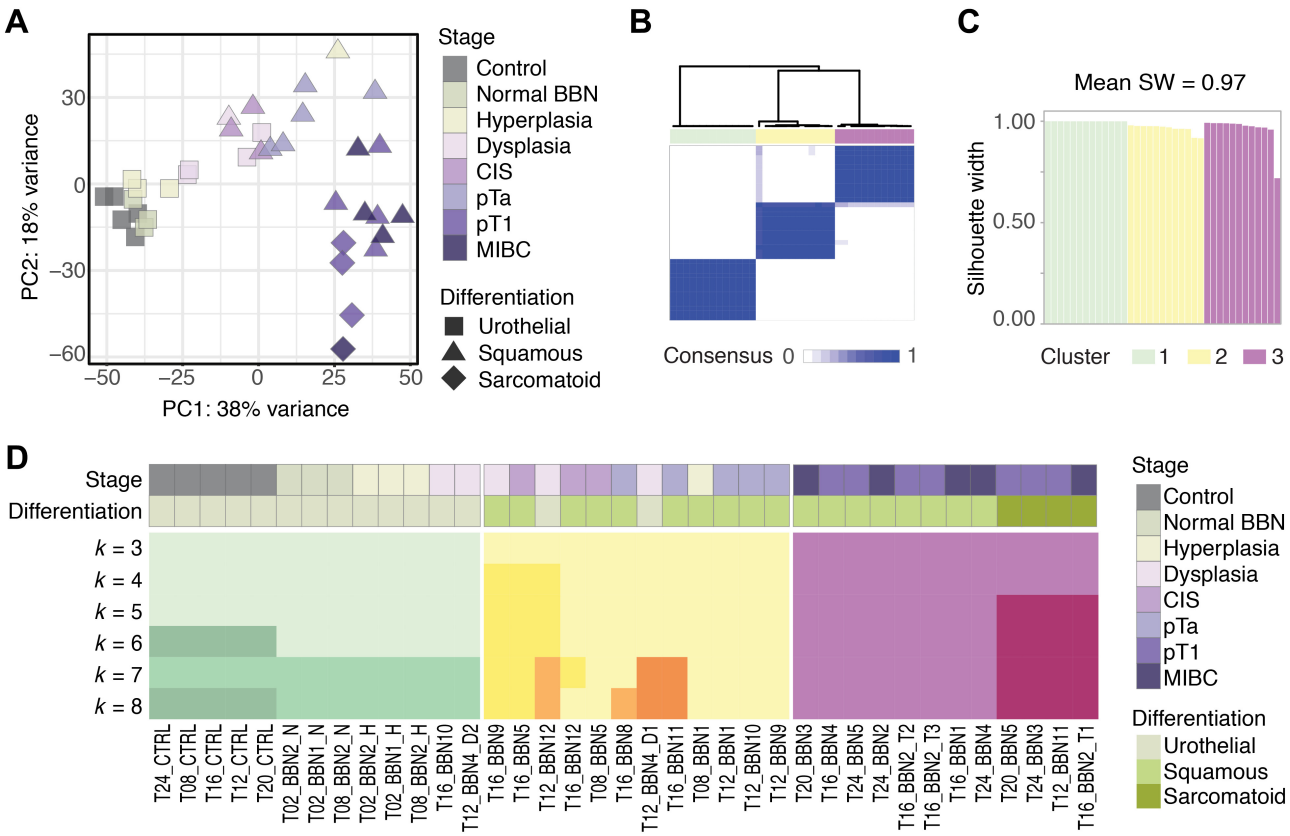

Figure 2. Transcriptomic progression groups in BBN-exposed mice are associated with morphological stage and differentiation. (A) Principal component analysis using the top 2,000 genes with most varying expression shows separation of samples according to stage along component 1 and according to differentiation along component 2. (B) Iterative hierarchical consensus clustering using the top 2,000 genes with most varying expression identified the $k = 3$ solution as the most stable grouping of BBN samples ('pam' clustering, 'ward.D2' linkage). (C) Silhouette plot metric shows high cohesion of each sample to its group. (D) Sample tracking plot showing grouping of BBN samples according to $k = 3$ to $k = 8$ solutions. In the $k = 3$ solution, samples are roughly grouped in control and pre-carcinogenic stages (green), non-infiltrating carcinogenic stages (yellow), and infiltrating tumors (purple). Starting at $k = 5$, infiltrating tumors were always separated according to differentiation (squamous versus sarcomatoid), regardless of stage (pT1 or MIBC). BBN, *N*-butyl-*N*-(4-hydroxybutyl)-nitrosamine; CIS, carcinoma *in situ*; MIBC, muscle-invasive bladder cancer.

tumors in human MIBCs [12,13]. PCA and clustering results indicated that BBN sarcomatoid cases may similarly represent a distinct group of progression. For our downstream analyses regarding molecular changes during progression, we thus considered the following sequential progression groups: (1) controls, (2) BBN-exposed urothelia with normal histology, (3) hyperplasia, (4) dysplasia, (5) CIS, (6) pTa, (7) infiltrating with squamous differentiation (≥pT1), and (8) infiltrating with sarcomatoid features (≥pT1).

Evolution of molecular subtyping during progression

We analyzed the evolution of molecular classifications during progression in our model using three classifiers [7,9,34]. As expected, all BBN-induced MIBC tumors, with squamous or sarcomatoid morphology, were classified as consensus Ba/Sq and BASE47 basal subtypes [17,21]. Strikingly, correlation to basal classes gradually increased during progression, transitioning to a full basal phenotype starting from the early stages of carcinogenesis (Figure 3A). LundTax confirmed and refined these observations. Most pTa tumours were assigned to the LundTax UroB group, which shares features of both urothelial-like (UroA) and Ba/Sq subtypes and is suggested to represent progression towards the basal phenotype [34,35]. Most infiltrating sarcomatoid cases (3/4) were classified as mesenchymal-like (Mes-like), indicating a distinct molecular phenotype.

Basal marker expression increased starting from the pre-malignant dysplasia stage, reaching maximum levels in infiltrating squamous samples (Figure 3B). However, infiltrating sarcomatoid cases had significantly lower expression of basal markers compared with cases with squamous divergence ($p = 8.1 \times 10^{-3}$) (Figure 3C). Conversely, luminal marker expression progressively decreased during progression, with a significant drop at basement membrane infiltration ($p = 0.01$) (Figure 3B,C). LundTax Mes-like infiltrating sarcomatoid cases displayed the highest levels of typical markers of human Mes-like tumors, *Vim* and *Zeb2*, with low expression of *Epcam* (Figure 3B,C) [8]. At the protein level, vimentin was expressed by tumor cells in sarcomatoid samples, whereas expression was identified in the stromal cells of non-sarcomatoid tumors with high *Vim* expression (Figure 3D). We also confirmed the sequential changes of

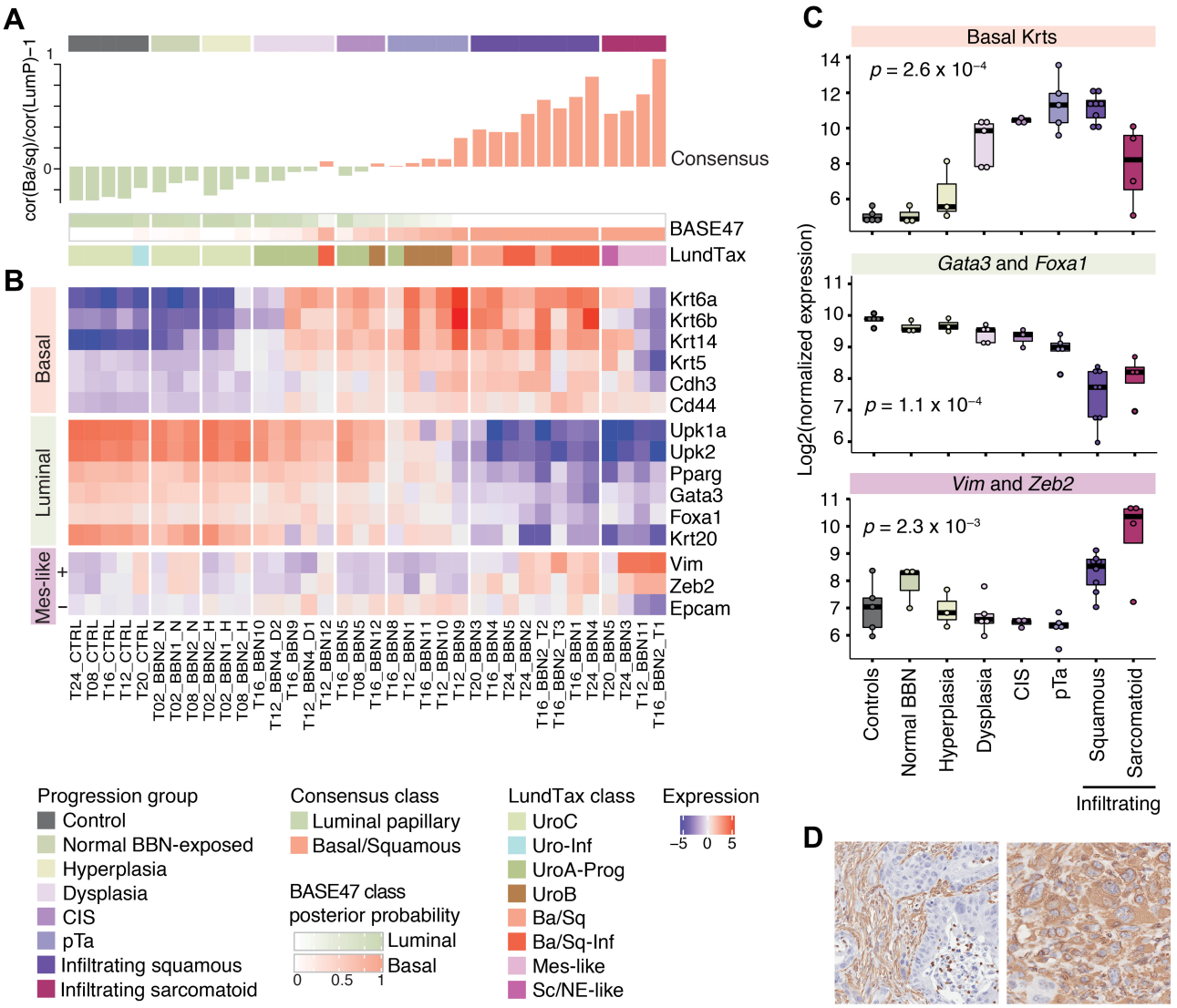

Figure 3. Molecular classification of BBN-induced lesions switches from luminal to basal during progression. (A) Molecular classification of each sample according to three classification systems: consensus, BASE47, and LundTax. A gradual increase in correlation to basal subtypes in the consensus and BASE47 systems was observed during progression. (B) Gene expression heatmap of markers of basal, luminal, and mesenchymal-like markers during progression. The color key represents row mean-centered values of log2-transformed normalized expression. (C) Dynamic expression profiles of mean basal keratins (*Krt6a*, *Krt6b*, *Krt5*, *Krt14*), luminal markers, and mesenchymal-like markers during progression. *P* values: two-sided Kruskal–Wallis test. (D) Representative images of vimentin IHC staining (brown) with hematoxylin counterstain. Vimentin staining is observed in the stroma of squamous tumors (left). In contrast, vimentin is expressed by the tumor cells in sarcomatoid tumors (right). BBN, *N*-butyl-*N*-(4-hydroxybutyl)-nitrosamine; CIS, carcinoma *in situ*; IHC, immunohistochemistry.

basal and luminal markers at the protein level by IHC on the complete cohort ($n = 40$ BBN-exposed mice) (supplementary material, Figure S3).

Overall, these findings indicated that early-stage tumors already exhibit basal characteristics and suggested that infiltrating sarcomatoid cases represent a distinct group of basal infiltrating BBN tumors with mesenchymal features.

Analysis of gene expression dynamics during progression identifies clusters of co-expressed genes with biological relevance

To identify patterns of gene expression changes during progression, we applied a time-course approach to our RNA-seq data using the Next maSigPro algorithm [36]. Setting our eight predefined progression stages as analysis time points, we identified 946 genes with significant temporal changes. Clustering of the significant genes distinguished five groups with similar patterns of expression changes during progression (Figure 4A,B). Clusters 1–3 of downregulated genes included genes known to play a role in urothelial differentiation (*Pparg*, *Grhl3*, uroplakins, *Krt20*, *Gata3*). The fourth cluster of genes with a coordinated increase starting from the dysplasia stage comprised basal markers (*Krt6a*, *Krt6b*, *Krt14*, *Cd44*, *Egfr*) as well as transcription factors reported to be active in the basal subtype (*Myc*, *Foxm1*, *Hif1a*) [7,11]. Cluster 5 grouped genes with low expression in early stages, such as *Vim* and *Cdkn2a*, which

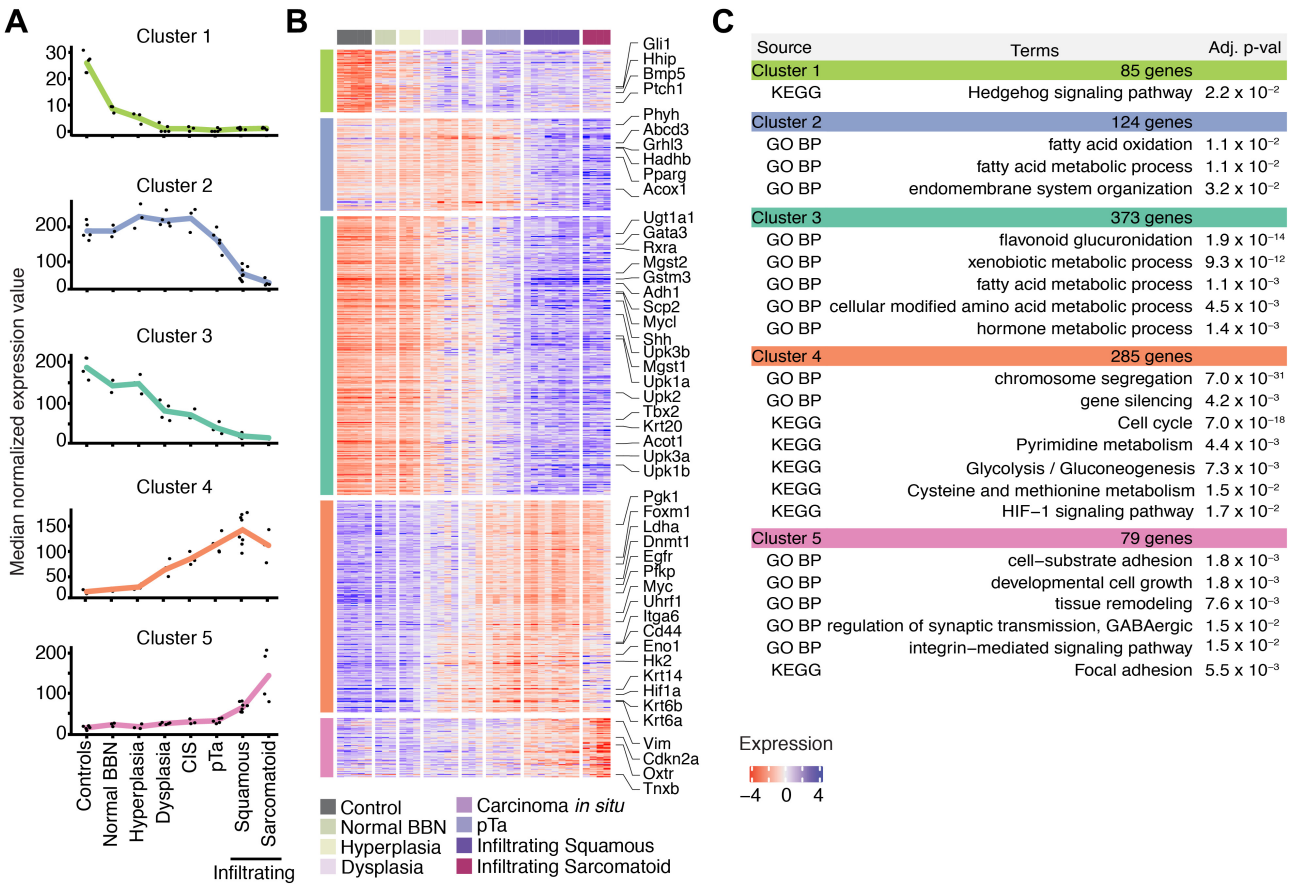

Figure 4. RNA-seq analysis using a time-course approach reveals distinct dynamic profiles of co-expressed genes during progression. (A) The 924 genes with significant temporal changes (Next maSigPro algorithm) were clustered into five distinct profiles of dynamic changes during progression. Clusters 1–3 (green, blue, and teal) represented successive waves of downregulation. Cluster 4 (orange) grouped genes with an upregulation in early stages of carcinogenesis leading to Ba/Sq invasive tumors. Genes in cluster 5 (pink) were upregulated at infiltration and were highest in sarcomatoid tumors. (B) Heatmap representation of the five clusters of genes with significant temporal changes during progression. Symbols of potential genes of interest in each cluster are shown. The color key represents row mean-centered values of log2-transformed normalized expression. (C) Overrepresentation analysis of the genes in each progression cluster using terms from the GO-BP and KEGG databases.

increased at infiltration and were highest in sarcomatoid cases.

We performed functional overrepresentation analysis of each cluster to identify implicated biological pathways (Figure 4C). Among expected processes, cell cycle and tissue remodeling terms were enriched in increasing clusters 4 and 5. Conversely, in downregulated clusters during progression, we identified genes of the canonical Hedgehog signaling pathway (*Gli1*, *Hhip*, *Ptch1*, *Shh*) and of xenobiotic detoxifying glucuronidation, in particular UDP-glucuronosyltransferase enzymes (*Ugt1a* genes in cluster 3), as previously reported [5,37]. Clusters 2 and 3 were both enriched in genes involved in fatty acid metabolism, in particular in oxidation (*Hadhb*, *Phyh*, *Abcd3*, *Pparg*). Concomitantly, glycolysis terms were enriched in cluster 4, linked to the upregulation of key enzymes or transporters of the glycolysis pathway (*Hk2*, *Pfkp*, *Pgk1*, *Eno1*, *Ldha*, *Slc16a1*). Cluster 4 also included *Hif1a* and *Myc*, known master regulators of glycolysis. These findings suggest an important energy rewiring during Ba/Sq bladder carcinogenesis.

A gene set with increasing expression during Ba/Sq carcinogenesis identifies NMBIC patients at risk of progression

We then explored the clinical relevance of cluster 4, a set of genes with a coordinated upregulation starting in early carcinogenic stages. We first investigated the expression of cluster 4 genes in different stages of human BLCA, using a publicly available dataset combining both NMBIC ($n = 213$) and MIBC ($n = 95$) samples [35]. Unsupervised hierarchical clustering using the expression of all human orthologs of cluster 4 genes distinguished two groups with distinct cluster 4 metagene scores (mean-centered expression of all cluster 4 genes), which were associated with stage (Figure 5A). Further investigation confirmed that cluster 4 metagene score significantly increased in a stepwise manner with stage in human tumors (Figure 5B). We then classified all NMBIC tumors in this cohort using a recent NMBIC classification scheme, comprising classes 1, 2a, 2b, and 3 [27]. Interestingly, nearly half (10/22) of the pTa tumors assigned to the cluster 4 metagene 'high' group

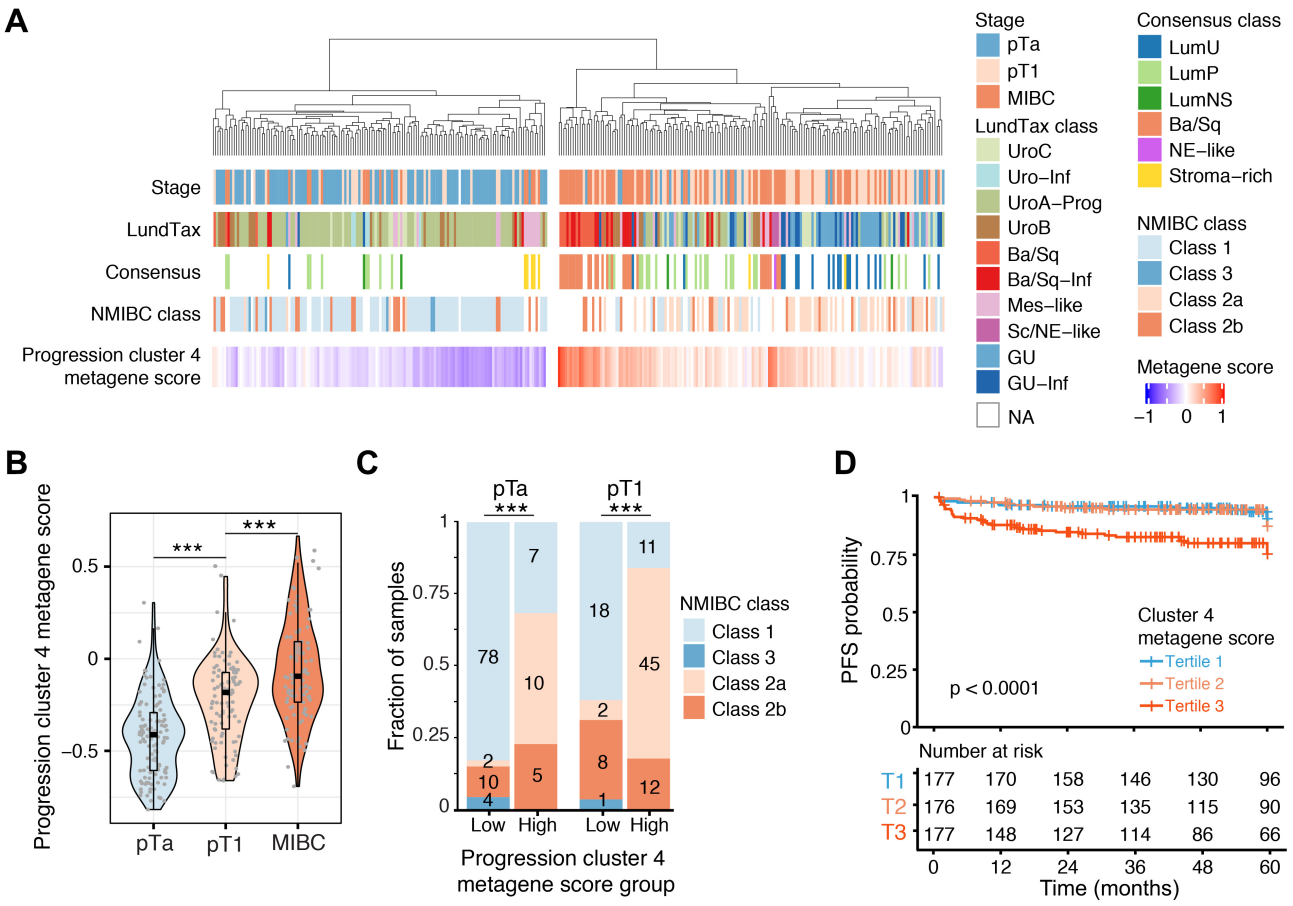

Figure 5. BBN progression cluster 4 shows relevance to human disease and identifies NMIBC patients at risk of progression. (A) Unsupervised consensus clustering using the expression of all human orthologs of BBN progression cluster 4 genes in a large dataset combining NMIBCs and MIBCs (Sjödahl 2012 cohort, $n = 308$) separated cluster 4 metagene-'low' samples, essentially composed of pTa tumors, from cluster 4 metagene-'high' tumors, mostly composed of pT1 and MIBCs. (B) Mean progression cluster 4 metagene score increased with stage in human tumors from the Sjödahl 2012 dataset ($n = 308$). ***$p < 0.001$, two-sided Wilcoxon test. (C) Proportion of NMIBC tumors (Sjödahl 2012 cohort, $n = 213$) in each NMIBC class according to the BBN cluster 4 metagene score group. ***$p < 0.001$, two-sided Fisher's exact test. (D) Kaplan–Meier curves of progression-free survival (PFS) probability when stratifying patients according to tertiles of cluster 4 metagene score values in the UROMOL NMIBC cohort ($n = 535$).

were classified as NMIBC class 2a, which is associated with the highest risk of progression (Figure 5C). These findings were confirmed in an additional cohort of both NMIBCs and MIBCs (CIT cohort, $n = 177$, supplementary material, Figure S4) [17]. In another NMIBC cohort ($n = 535$, UROMOL project) [27], progression cluster 4 metagene score was significantly higher in pT1 than in pTa tumors ($p = 1.7 \times 10^{-10}$, supplementary material, Figure S3D). Cluster 4 gene expression level was associated with progression-free survival in this cohort and patients with the highest score had the worst outcome (log-rank $p < 0.0001$, Figure 5D).

BBN sarcomatoid tumors show relevance to human sarcomatoid variant

Since sarcomatoid BBN-induced tumors in mice have not been extensively described in the literature, we further explored their transcriptomes. We first performed differential gene expression analysis between infiltrating sarcomatoid and non-sarcomatoid samples (supplementary material, Figure S5A). Top enriched terms in the upregulated genes included migration, matrix adhesion, and mesenchymal cell differentiation, whereas downregulated genes were enriched in terms associated with epithelial cell differentiation and cell–cell adhesion (supplementary material, Figure S5B), suggesting epithelial–mesenchymal transition (EMT) features. Supporting these findings, the Hallmark EMT gene set was within the top enriched pathways in gene set enrichment analysis (GSEA) (supplementary material, Figure S5C,D). To test if BBN-induced sarcomatoid cases recapitulate the gene expression profile of the sarcomatoid variant of human MIBC, we explored the gene expression profiles of a cohort of 112 patients with urothelial carcinoma, including 28 of the sarcomatoid variant [12]. Guo *et al* human sarcomatoid cases were similar to BBN sarcomatoid samples regarding molecular classification (Figure 6A). We then sought to compare the candidate mechanisms involved in BBN sarcomatoid phenotype with those of human sarcomatoid samples. We thus classified all 112 human

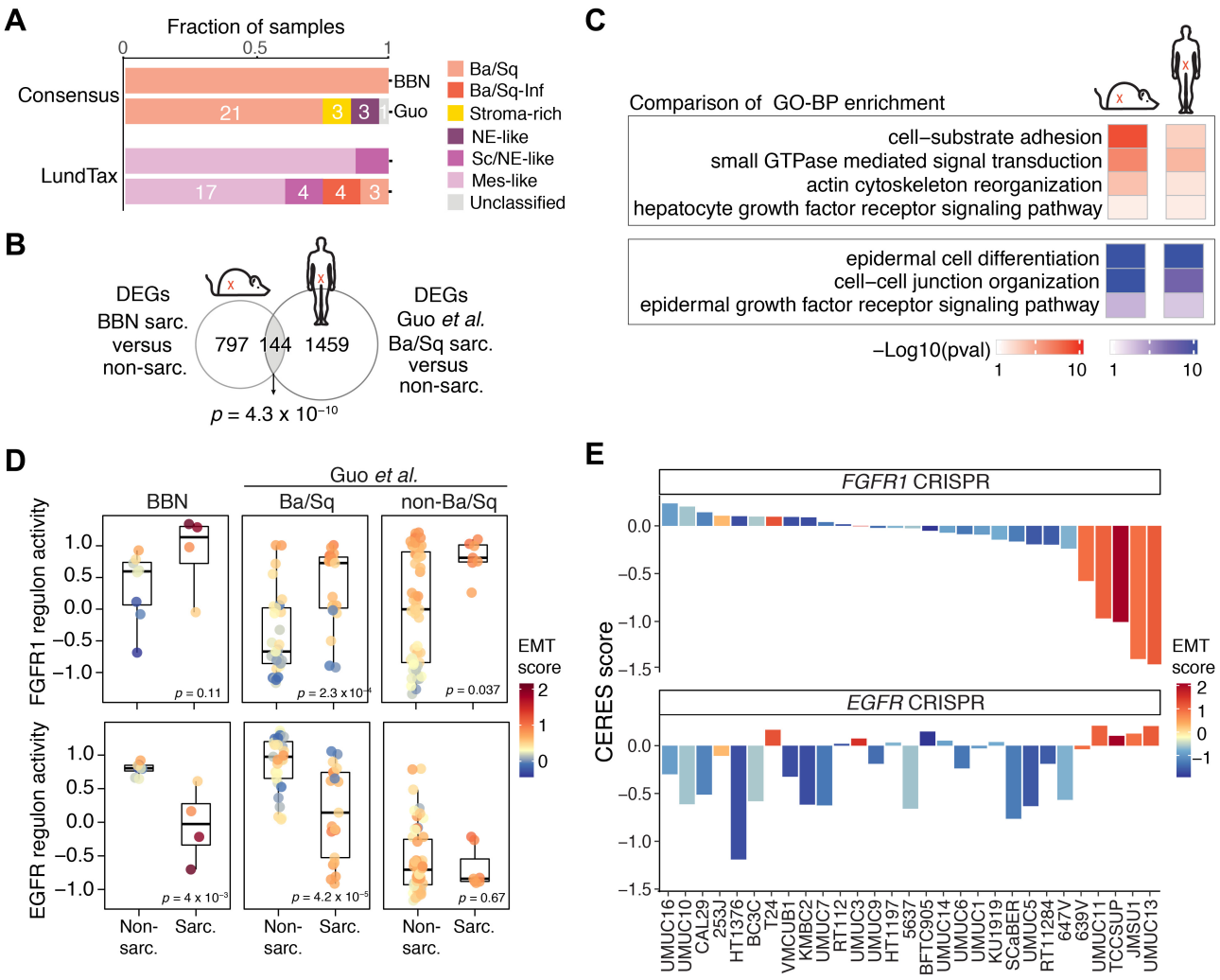

Figure 6. BBN-induced sarcomatoid tumors resemble the human counterpart and reveal an EGFR to FGFR1 switch with sarcomatoid dedifferentiation. (A) Molecular classes of BBN and human sarcomatoid tumors (Guo *et al* cohort, $n = 28$) according to the consensus and LundTax systems. (B) Significant overlap in differentially expressed genes (DEGs) between BBN sarcomatoid ($n = 4$) and non-sarcomatoid ($n = 8$) infiltrating samples and human Ba/Sq sarcomatoid ($n = 21$) versus Ba/Sq non-sarcomatoid samples ($n = 29$). *P* value: one-sided Fisher's exact test using all orthologs identified in the BBN cohort as background genes. (C) Functional overrepresentation analysis with GO-BP gene sets, using up- (red) or down-regulated (blue) genes between sarcomatoid and non-sarcomatoid samples shows common dysregulated pathways in BBN and human sarcomatoid tumors, which are related to epithelial–mesenchymal transition (EMT). (D) Comparison of EGFR and FGFR1 regulon activity between sarcomatoid and non-sarcomatoid samples in our BBN cohort and in human samples [Guo *et al* with Ba/Sq ($n = 50$) and non-Ba/Sq ($n = 62$) tumors]. *P* value: two-sided Wilcoxon test. (E) The effect of *FGFR1* and *EGFR* knockout in bladder cancer cell lines ($n = 29$, Achilles Project, Broad Institute) is associated with EMT score.

samples using the consensus classifier, identifying 50 Ba/Sq tumors. We then performed differential gene expression analysis between Ba/Sq sarcomatoid ($n = 21$) and Ba/Sq non-sarcomatoid cases ($n = 29$). A significant overlap was found between the dysregulated genes identified in BBN compared with human samples (Figure 6B). Comparison of functional enrichment associated with the observed dysregulated genes revealed common biological processes (Figure 6C). Both datasets pointed to terms related to EMT as well as to downregulation of EGFR signaling in sarcomatoid samples. To compare the changes in EMT in mouse and human tumors, we calculated a previously published EMT score [32] in both our BBN and Ba/Sq human samples. Sarcomatoid cases had a significantly higher EMT score than non-sarcomatoid samples in both datasets (supplementary material, Figure S6A), further demonstrating the EMT profile of sarcomatoid tumors in our model and its relevance to the human sarcomatoid variant.

An EGFR to FGFR1 signaling switch occurs with sarcomatoid dedifferentiation

To further confirm the downregulation of EGFR signaling in sarcomatoid samples in our BBN cohort, we calculated the activity of 22 regulators associated with BLCA, including EGFR [11]. EGFR regulon was significantly downregulated in BBN sarcomatoid compared with non-sarcomatoid infiltrating cases (Figure 6D). By computing all 22 regulons, we observed that FGFR1 displayed high activity in sarcomatoid cases (supplementary material, Figure S6B). GSEA using ranked fold-changes of FGFR1

target genes between BBN sarcomatoid and non-sarcomatoid samples confirmed the significant enrichment of FGFR1 regulon in sarcomatoid cases (adj. $p = 2.4 \times 10^{-3}$) (supplementary material, Figure S6C). However, the mean FGFR1 regulon activity score was not significantly higher in infiltrating sarcomatoid compared with non-sarcomatoid cases, potentially owing to the low number of BBN samples (Figure 6D). We thus similarly calculated regulon activity scores in the Guo *et al* cohort ($n = 112$) and confirmed the EGFR/FGFR1 switch in human Ba/Sq sarcomatoid samples, but not in non-Ba/Sq sarcomatoid cases (Figure 6D and supplementary material, Figure S6D).

Given the previously reported role of FGFR1 in EMT [38], we interrogated the association of FGFR1 activity and EMT score in BBN and human tumors. Interestingly, FGFR1 regulon activity was positively correlated with EMT score in both Ba/Sq and non-Ba/Sq samples ($R = 0.83$, $p = 9.1 \times 10^{-14}$ in Ba/Sq and $R = 0.88$, $p < 2.2 \times 10^{-16}$ in non-Ba/Sq from the Guo *et al* cohort; $R = 0.82$, $p = 0.001$ in our BBN cohort). In contrast, EGFR regulon activity was negatively correlated with EMT in both mouse and Ba/Sq human cohorts, but not in non-Ba/Sq human samples (supplementary material, Figure S6E,F). *FGFR1* expression alone was also highly correlated with EMT score in a larger MIBC dataset (TCGA, $n = 408$, $R = 0.82$, $p < 2.2 \times 10^{-16}$) as well as in BLCA cell lines (CCLE, $n = 36$, $R = 0.85$, $p = 6.9 \times 10^{-11}$), suggesting a stroma-independent *FGFR1* expression (supplementary material, Figure S6G,H).

Sensitivity to *FGFR1* knockout was significantly correlated with both *FGFR1* expression and EMT score in BLCA cell lines (supplementary material, Figure S6I,J) in a genome-wide CRISPR screen ($n = 29$, Achilles Project, Broad Institute). As previously suggested [39,40], *EGFR* knockout had no effect on viability in cell lines with the highest EMT scores, including in cells with the highest sensitivity to *FGFR1* inhibition (Figure 6E). Of note, EMT-high cell lines that were not sensitive to *FGFR1* inhibition harbor activating *RAS* mutations, suggesting potentially overlapping downstream pathways.

Taken together, these data show that sarcomatoid dedifferentiation, characterized by EMT, is associated with an EGFR to FGFR1 signaling switch, with potential sensitivity to FGFR1 inhibition.

Discussion

The inherent natural history of the aggressive Ba/Sq BLCA subtype hampers the study of progression from early-stage carcinoma to Ba/Sq MIBC in human samples. Here, we performed laser-capture microdissection and RNA-seq of lesions at all stages of carcinogenesis in a murine model of Ba/Sq MIBC to study gene expression dynamics during progression.

In human carcinogenesis, molecular subtype changes during progression from NMIBC to MIBC have not been fully elucidated, in particular in the Ba/Sq subtype. To address this question, Sjödhal *et al* built a cohort of 73 patients with NMIBC who eventually progressed to MIBC [19]. Only six patients had recurring NMIBC that eventually progressed to Ba/Sq MIBC, illustrating the challenge of studying molecular dynamics in this subtype particularly. In our study, gene expression-based classifications revealed that early stages already displayed Ba/Sq features. These findings are in line with lineage tracing studies in mice showing that basal Krt5/Shh-expressing cells give rise to CIS and invasive tumors in the BBN-induced model [5,6]. Using single-cell transcriptome profiling and FACS analysis of pre-sorted and cultured BBN-induced tumor cells, Sfakianos *et al* identified co-expression of luminal and basal genes at the single-cell level and demonstrated cell lineage plasticity [41]. These observations suggest that a subtype switch could occur with progression.

In contrast to BBN-induced mouse CIS, human CIS with basal features is a rare finding. In fact, the majority of human CIS cases are characterized by the aberrant overexpression of the luminal marker KRT20. However, cases of CIS expressing basal markers have been reported [18,42]. NMIBCs displaying a basal IHC phenotype have also been reported and were suggested to be associated with progression, although these findings are controversial [43–45]. While human Ba/Sq MIBCs may arise after a molecular phenotype switch, our study suggests that a subset could evolve from true Ba/Sq CIS. This hypothesis is supported by a study suggesting that basal subtype commitment already occurs at the stage of CIS [46], as well as by mucosal field-effect studies demonstrating clonal relationships between CIS and invasive tumors and revealing a basal-specific field effect in basal tumors [47,48].

Functionally related genes tend to show correlated expression patterns across multiple conditions or perturbations [49]. To investigate the gene expression changes during progression, we thus used a unique approach by deriving a time-course RNA-seq data algorithm. The time-course approach identified sets of genes with similar co-expression patterns during progression. Validating this method, we identified previously reported pathway dysregulations, such as Shh and glucoronidation pathway downregulation [5,37], or expected pathways such as cell cycle upregulation. This analysis also suggested that a metabolism rewiring occurs in the early steps of Ba/Sq carcinogenesis, towards anaerobic glycolysis. Fantini *et al* performed RNA-seq of five BBN-induced MIBCs and three pre-tumoural lesions at 4 weeks of exposure and identified metabolic changes in established tumors but not in pre-tumoral samples [21]. However, by using laser microdissection of pre-tumoral lesions in our study, enrichment in tumor-cell RNA likely allowed us to capture such changes with more sensitivity.

We acknowledge certain limitations related to our study design. We are aware that this analysis represents a pseudo-time series, where each sample is in fact a snapshot of a static state. However, the BBN-induced carcinogenesis is a stable model in which mice, with the

same genetic background, inevitably develop MIBC as carcinogenic exposure increases. Additionally, to preserve the tissue, we did not exhaust each FFPE block and thus could not control whether the laser-capture microdissected area was in fact the highest-stage lesion in the entire mouse bladder.

Finally, we also report here, to our best knowledge, the first molecular characterization of BBN-induced sarcomatoid tumors in mice. BBN-induced sarcomatoid tumors, like human sarcomatoid BLCA, were assigned to the Ba/Sq subtype and harbored features of EMT [12,13], suggesting that BBN-induced sarcomatoid tumors recapitulate the transcriptional features of human sarcomatoid BLCA, broadening the utility of the BBN model to studies focusing on this variant.

Through differential analysis between sarcomatoid and non-sarcomatoid tumors, we demonstrated that an EGFR/FGFR1 switch occurs with sarcomatoid dedifferentiation in both BBN-induced and human Ba/Sq tumors. FGFR1-mediated EMT has been shown in other cancer types [50,51]. In BLCA, FGFR1 overexpression has previously been reported in a subset of cases [52,53], 52,53], and others have demonstrated that FGFR1 expression in BLCA cell lines induced EMT phenotypic changes [38]. Here, we have shown that BLCA cell lines with the highest EMT scores and FGFR1 expression were the most sensitive to FGFR1 inhibition. These findings are in line with those of Tomlinson *et al* [52], who showed that EMT-high JMSU1 cells were sensitive to an FGFR inhibitor. Further *in vivo* studies should investigate whether FGFR inhibitors alone or in combination with other therapies could tackle the biological complexity of sarcomatoid BLCA.

Overall, our findings provide insights into the underlying biology of Ba/Sq BLCA progression and sarcomatoid dedifferentiation with potential clinical implications.

Acknowledgements

We would like to thank Elodie Chapeaublanc for her assistance in data management and GEO submission, and Clémentine Krucker for digital histology slide data management. This work was supported by a grant from Ligue Nationale Contre le Cancer (JF, LC, YA, FR IBP) as an associated team (Equipe labellisée); the 'Carte d'Identité des Tumeurs' program initiated, developed, and funded by Ligue Nationale Contre le Cancer; and by the French Institut National du Cancer INCa (PRT-K 2013, Programme de Recherche Translationnelle en Cancérologie, 'DIATRIBBE'). JF was supported by the Fondation ARC pour la recherche sur le cancer and by Groupe Pasteur Mutualité. LC was supported by the Fondation Médicale pour la Recherche. High-throughput sequencing was performed by the ICGex NGS platform of the Institut Curie supported by the grants ANR-10-EQPX-03 (Equipex) and ANR-10-INBS-09-08 (France Génomique Consortium) from the Agence Nationale de la Recherche ('Investissements d'Avenir' program), by the ITMO-Cancer Aviesan (Plan Cancer III), and by the SiRIC-Curie program (SiRIC Grants INCa-DGOS-465 and INCa-DGOS-Inserm_12554).

Author contributions statement

JF participated in the study design, performed laser-capture microdissection, RNA extraction and histological, immunohistochemical and RNA-seq analyses and drafted the manuscript. JW participated in the study design, RNA extraction, IHC analysis and performed the RNA-seq pre-processing. LC participated in the RNA-seq data analysis. HN-K participated in the study design. NK and PM performed the immunohistochemistry experiments. AR and DG performed the RNA-seq libraries. SB generated the RNA-seq data. MS and YA participated in the histological and immunohistochemistry analysis. IB-P, FR and YA conceptualized and supervised the study and revised the manuscript. All authors read and approved the final manuscript.

Data availability statement

Generated RNA-seq data have been deposited in the Gene Expression Omnibus (GEO; https://www.ncbi.nlm.nih.gov/geo/query/acc.cgi) and are publicly available under accession number GSE197016. Details on the public data analyzed are provided in Supplementary materials and methods.

References

1. Bray F, Ferlay J, Soerjomataram I, *et al*. Global cancer statistics 2018: GLOBOCAN estimates of incidence and mortality worldwide for 36 cancers in 185 countries. *CA Cancer J Clin* 2018; **68:** 394–424.
2. Humphrey PA, Moch H, Cubilla AL, *et al*. The 2016 WHO classification of tumours of the urinary system and male genital organs – part B: prostate and bladder tumours. *Eur Urol* 2016; **70:** 106–119.
3. Babjuk M, Burger M, Compérat EM, *et al*. European Association of Urology guidelines on non-muscle-invasive bladder cancer (TaT1 and carcinoma *in situ*) – 2019 update. *Eur Urol* 2019; **76:** 639–657.
4. Knowles MA, Hurst CD. Molecular biology of bladder cancer: new insights into pathogenesis and clinical diversity. *Nat Rev Cancer* 2015; **15:** 25–41.
5. Shin K, Lim A, Odegaard JI, *et al*. Cellular origin of bladder neoplasia and tissue dynamics of its progression to invasive carcinoma. *Nat Cell Biol* 2014; **16:** 469–478.
6. Van Batavia J, Yamany T, Molotkov A, *et al*. Bladder cancers arise from distinct urothelial sub-populations. *Nat Cell Biol* 2014; **16:** 982–991.
7. Kamoun A, de Reyniès A, Allory Y, *et al*. A consensus molecular classification of muscle-invasive bladder cancer. *Eur Urol* 2020; **77:** 420–433.
8. Sjödahl G, Eriksson P, Liedberg F, *et al*. Molecular classification of urothelial carcinoma: global mRNA classification versus tumour-cell phenotype classification. *J Pathol* 2017; **242:** 113–125.

9. Damrauer JS, Hoadley KA, Chism DD, *et al*. Intrinsic subtypes of high-grade bladder cancer reflect the hallmarks of breast cancer biology. *Proc Natl Acad Sci U S A* 2014; **111:** 3110–3115.
10. Choi W, Porten S, Kim S, *et al*. Identification of distinct basal and luminal subtypes of muscle-invasive bladder cancer with different sensitivities to frontline chemotherapy. *Cancer Cell* 2014; **25:** 152–165.
11. Robertson AG, Kim J, Al-Ahmadie H, *et al*. Comprehensive molecular characterization of muscle-invasive bladder cancer. *Cell* 2017; **171:** 540–556.e25.
12. Guo CC, Majewski T, Zhang L, *et al*. Dysregulation of EMT drives the progression to clinically aggressive sarcomatoid bladder cancer. *Cell Rep* 2019; **27:** 1781–1793.e4.
13. Genitsch V, Kollár A, Vandekerkhove G, *et al*. Morphologic and genomic characterization of urothelial to sarcomatoid transition in muscle-invasive bladder cancer. *Urol Oncol* 2019; **37:** 826–836.
14. Lopez-Beltran A, Henriques V, Montironi R, *et al*. Variants and new entities of bladder cancer. *Histopathology* 2019; **74:** 77–96.
15. Lerner SP, McConkey DJ, Hoadley KA, *et al*. Bladder cancer molecular taxonomy: summary from a consensus meeting. *Bladder Cancer* 2016; **2:** 37–47.
16. Hardy CSC, Ghaedi H, Slotman A, *et al*. Immunohistochemical assays for bladder cancer molecular subtyping: optimizing parsimony and performance of Lund taxonomy classifiers. *J Histochem Cytochem* 2022; **70:** 357–375.
17. Rebouissou S, Bernard-Pierrot I, de Reyniès A, *et al*. EGFR as a potential therapeutic target for a subset of muscle-invasive bladder cancers presenting a basal-like phenotype. *Sci Transl Med* 2014; **6:** 244ra91.
18. Barth I, Schneider U, Grimm T, *et al*. Progression of urothelial carcinoma *in situ* of the urinary bladder: a switch from luminal to basal phenotype and related therapeutic implications. *Virchows Arch* 2018; **472:** 749–758.
19. Sjödahl G, Eriksson P, Patschan O, *et al*. Molecular changes during progression from nonmuscle invasive to advanced urothelial carcinoma. *Int J Cancer* 2020; **146:** 2636–2647.
20. Vasconcelos-Nóbrega C, Colaço A, Lopes C, *et al*. BBN as an urothelial carcinogen. *In Vivo* 2012; **26:** 727–739.
21. Fantini D, Glaser AP, Rimar KJ, *et al*. A carcinogen-induced mouse model recapitulates the molecular alterations of human muscle invasive bladder cancer. *Oncogene* 2018; **37:** 1911–1925.
22. Dobin A, Davis CA, Schlesinger F, *et al*. STAR: ultrafast universal RNA-seq aligner. *Bioinformatics* 2013; **29**: 15–21.
23. Liao Y, Smyth GK, Shi W. The Subread aligner: fast, accurate and scalable read mapping by seed-and-vote. *Nucleic Acids Res* 2013; **41**: e108.
24. R Core Team. *R: A language and environment for statistical computing*. R Foundation for Statistical Computing: Vienna, Austria, 2020.
25. Wilkerson MD, Hayes DN. ConsensusClusterPlus: a class discovery tool with confidence assessments and item tracking. *Bioinformatics* 2010; **26:** 1572–1573.
26. Durinck S, Spellman PT, Birney E, *et al*. Mapping identifiers for the integration of genomic datasets with the R/Bioconductor package biomaRt. *Nat Protoc* 2009; **4**: 1184–1191.
27. Lindskrog SV, Prip F, Lamy P, *et al*. An integrated multi-omics analysis identifies prognostic molecular subtypes of non-muscle-invasive bladder cancer. *Nat Commun* 2021; **12:** 2301.
28. Yu G, Wang L-G, Han Y, *et al*. clusterProfiler: an R package for comparing biological themes among gene clusters. *OMICS* 2012; **16**: 284–287.
29. Yu G, He Q-Y. ReactomePA: an R/Bioconductor package for reactome pathway analysis and visualization. *Mol Biosyst* 2016; **12**: 477–479.
30. Love MI, Huber W, Anders S. Moderated estimation of fold change and dispersion for RNA-seq data with DESeq2. *Genome Biol* 2014; **15**: 550.
31. Ritchie ME, Phipson B, Wu D, *et al*. limma powers differential expression analyses for RNA-sequencing and microarray studies. *Nucleic Acids Res* 2015; **43**: e47.
32. de Reyniès A, Jaurand MC, Renier A, *et al*. Molecular classification of malignant pleural mesothelioma: identification of a poor prognosis subgroup linked to the epithelial-to-mesenchymal transition. *Clin Cancer Res* 2014; **20:** 1323–1334.
33. Ohtani M, Kakizoe T, Nishio Y, *et al*. Sequential changes of mouse bladder epithelium during induction of invasive carcinomas by *N*-butyl-*N*-(4-hydroxybutyl)nitrosamine. *Cancer Res* 1986; **46:** 2001–2004.
34. Marzouka NAD, Eriksson P, Rovira C, *et al*. A validation and extended description of the Lund taxonomy for urothelial carcinoma using the TCGA cohort. *Sci Rep* 2018; **8:** 3737.
35. Sjödahl G, Lauss M, Lövgren K, *et al*. A molecular taxonomy for urothelial carcinoma. *Clin Cancer Res* 2012; **18:** 3377–3386.
36. Nueda MJ, Tarazona S, Conesa A. Next maSigPro: updating maSigPro bioconductor package for RNA-seq time series. *Bioinformatics* 2014; **30:** 2598–2602.
37. Iida K, Mimura J, Itoh K, *et al*. Suppression of AhR signaling pathway is associated with the down-regulation of UDP-glucuronosyltransferases during BBN-induced urinary bladder carcinogenesis in mice. *J Biochem* 2010; **147:** 353–360.
38. Tomlinson DC, Baxter EW, Loadman PM, *et al*. FGFR1-induced epithelial to mesenchymal transition through MAPK/PLCγ/COX-2-mediated mechanisms. *PLoS One* 2012; **7:** e38972.
39. Black PC, Brown GA, Inamoto T, *et al*. Sensitivity to epidermal growth factor receptor inhibitor requires E-cadherin expression in urothelial carcinoma cells. *Clin Cancer Res* 2008; **14:** 1478–1486.
40. Shrader M, Pino MS, Brown G, *et al*. Molecular correlates of gefitinib responsiveness in human bladder cancer cells. *Mol Cancer Ther* 2007; **6:** 277–285.
41. Sfakianos JP, Daza J, Hu Y, *et al*. Epithelial plasticity can generate multi-lineage phenotypes in human and murine bladder cancers. *Nat Commun* 2020; **11:** 2540.
42. Guo CC, Fine SW, Epstein JI. Noninvasive squamous lesions in the urinary bladder: a clinicopathologic analysis of 29 cases. *Am J Surg Pathol* 2006; **30:** 883–891.
43. Jackson CL, Chen L, Hardy CSC, *et al*. Diagnostic and prognostic implications of a three-antibody molecular subtyping algorithm for non-muscle invasive bladder cancer. *J Pathol Clin Res* 2022; **8:** 143–154.
44. Rebola J, Aguiar P, Blanca A, *et al*. Predicting outcomes in non-muscle invasive (Ta/T1) bladder cancer: the role of molecular grade based on luminal/basal phenotype. *Virchows Arch* 2019; **475:** 445–455.
45. Muilwijk T, Akand M, Van der Aa F, *et al*. Cytokeratin 5 and cytokeratin 20 inversely correlate with tumour grading in Ta non-muscle-invasive bladder cancer. *J Cell Mol Med* 2021; **25:** 7890–7900.
46. Wullweber A, Strick R, Lange F, *et al*. Bladder tumor subtype commitment occurs in carcinoma *in situ* driven by key signaling pathways including ECM remodeling. *Cancer Res* 2021; **81:** 1552–1566.
47. Bondaruk J, Jaksik R, Wang Z, *et al*. The origin of bladder cancer from mucosal field effects. *iScience* 2022; **25:** 104551.
48. Lawson ARJ, Abascal F, Coorens THH, *et al*. Extensive heterogeneity in somatic mutation and selection in the human bladder. *Science* 2020; **370:** 75–82.
49. Stuart JM, Segal E, Koller D, *et al*. A gene-coexpression network for global discovery of conserved genetic modules. *Science* 2003; **302:** 249–255.
50. Acevedo VD, Gangula RD, Freeman KW, *et al*. Inducible FGFR-1 activation leads to irreversible prostate adenocarcinoma and an epithelial-to-mesenchymal transition. *Cancer Cell* 2007; **12:** 559–571.
51. Nguyen PT, Tsunematsu T, Yanagisawa S, *et al*. The FGFR1 inhibitor PD173074 induces mesenchymal–epithelial transition through the transcription factor AP-1. *Br J Cancer* 2013; **109:** 2248–2258.
52. Tomlinson DC, Lamont FR, Shnyder SD, *et al*. Fibroblast growth factor receptor 1 promotes proliferation and survival via activation of the

mitogen-activated protein kinase pathway in bladder cancer. *Cancer Res* 2009; **69:** 4613–4620.
53. Lim S, Koh MJ, Jeong HJ, *et al*. Fibroblast growth factor receptor 1 overexpression is associated with poor survival in patients with resected muscle invasive urothelial carcinoma. *Yonsei Med J* 2016; **57:** 831–839.
54. Espina V, Wulfkuhle JD, Calvert VS, *et al*. Laser-capture microdissection. *Nat Protoc* 2006; **1:** 586–603.
55. Castro MAA, de Santiago I, Campbell TM, *et al*. Regulators of genetic risk of breast cancer identified by integrative network analysis. *Nat Genet* 2015; **48:** 12–21.
56. Meyers RM, Bryan JG, McFarland JM, *et al*. Computational correction of copy number effect improves specificity of CRISPR–Cas9 essentiality screens in cancer cells. *Nat Genet* 2017; **49:** 1779–1784.

References 54–56 are cited only in the supplementary material.

SUPPLEMENTARY MATERIAL ONLINE

Supplementary materials and methods

Figure S1. Representative images of BBN-induced bladder flat non-invasive lesions and proliferation rate

Figure S2. Representative images of BBN-induced bladder lesions of different stages of carcinogenesis before and after laser-capture microdissection

Figure S3. Expression patterns of basal and luminal markers during progression in BBN-exposed mice

Figure S4. BBN progression cluster 4 shows relevance to human disease

Figure S5. Differential gene expression analysis between sarcomatoid and non-sarcomatoid infiltrating BBN samples

Figure S6. FGFR1 regulon, expression, and knockout effect are associated with EMT, which is increased in sarcomatoid tumors